第 43 卷 第 16 期/2023 年 8 月/光学学报 研究论文

光学学报

基于石墨烯超表面的可调谐慢光特性研究

马毅[1,2]，郭靖宇[1,2]，陈麟[1,2*]

[1]上海理工大学光电信息科学与计算机工程学院，上海 200093；

[2]上海市现代光学系统重点实验室，上海 200093

摘要 基于金属-石墨烯耦合的开口谐振环超材料，在0.8～1.2 THz范围成功实现等离诱导透明效应(PIT)。通过调节石墨烯的费米能级可以在0.929 THz和1.037 THz处实现振幅调制，最大调制深度分别为96.05%和65.40%。通过提出等效电容耦合结构来量化偏置电压与石墨烯费米能级的关系，该结构在慢光应用的研究结果表明，当偏置电压为30 V，石墨烯宽度为2 μm时，群延时、群折射率、延时带宽积和Q值分别可达93.12 ps，756.67，9.31，10.19。该研究结果对可调谐慢光器件的应用具有潜在的推动作用。

关键词 等离诱导透明；石墨烯；可调谐；慢光效应；太赫兹

中图分类号 O439 **文献标志码** A **DOI**：10.3788/AOS230810

1 引 言

太赫兹(THz)频率范围在0.1～10 THz，处于微波和红外波段之间。因其具有能量低、穿透性强、信噪比高等优点，被广泛应用于生物传感、医学诊断、成像等领域[1-3]。超材料(MM)是指由人工设计的具有超常物理性质的周期性结构，在亚波长尺寸成像、电磁波吸收以及光学传感等领域应用广泛[4-8]。太赫兹波能够实现对超材料的调控作用，近年来超材料已经为电磁功能器件设计提供了新思路。由于功能固定的超材料在实际应用的局限性，可以在设计中加入可调材料，例如半导体[9]、液晶[10]、相变材料[11]，以及二维(2D)材料石墨烯[12-15]等，他们的导电或电介质属性可以通过外界热、光或者电刺激控制。石墨烯作为一种拥有独特光学性质的二维半导体材料，其可以通过外加激励如光、电或者直接掺杂载流子改变费米能级进而改变其电导率。2015年，Zhao等[16]提出了一种开口谐振环与方形石墨烯耦合的结构。其中，石墨烯薄膜作为明模式，开口谐振环作为暗模式，两个模式干涉相消成功实现了电磁诱导透明效应且能够通过改变费米能级的大小对窗口实现调制。2020年，Peng等[17]提出了一种非对称双椭圆结构，通过改变费米能级得到了70%的调制深度，Fano共振峰值达到0.918。

表面等离激元(SPPs)是电磁波与金属相互作用时在交界处产生电子振荡的现象，其中局域性SPPs常常伴随着Fano谐振、等离诱导透明效应(PIT)等现象产生[18]，在透射峰处会产生大的色散从而使电磁波群速度减慢。这种现象被称作慢光效应，在光开关、光存储和非线性光学等方面具有潜在的应用价值[19-21]。由于金属SPPs的性能主要由几何参数决定，且金属阵列因欧姆损耗而消耗能量太多，因此器件的实用价值较低。石墨烯作为一种可动态调控的二维材料，在太赫兹频段也能激发SPPs，且石墨烯的欧姆损耗很低，因此在超表面设计中加入石墨烯不仅符合集成小型化方面要求，还能使器件具有动态可调性从而符合多种应用场景，这使得太赫兹器件发展与应用具有重大意义。

本文提出了一种金属-石墨烯耦合的多重开口谐振环(SRR)结构，电磁波垂直射入超表面并在交界处激发SPPs，该结构的两个子谐振器能够产生明-明模耦合从而产生PIT效应。相比于金属材料的PIT，石墨烯能够通过外加偏置电压调控费米能级从而实现PIT效应动态可调。由于PIT透射峰处会产生较大的色散，该结构可用于慢光存储且相较于其他研究具有显著的优势。

2 结构设计与仿真方法

所设计的动态可调的慢光器结构如图1所示，该结构由三层构成：最下面是介电常数ε=11.7的蓝宝石衬底，其厚度为28 μm；中间为一层聚酰亚胺绝缘层，其介电常数ε=3.5；最上层为两个SRR结构嵌套

收稿日期：2023-04-13；**修回日期**：2023-04-23；**录用日期**：2023-05-06；**网络首发日期**：2023-05-16

基金项目：国家自然科学基金(61988102，62275157)、上海市教育发展基金会“曙光计划”(18SG44)、高等学校学科创新引智计划(D18014)

通信作者：*linchen@usst.edu.cn

放置，其材料为电导率为 4.516×10^7 S/m 的金薄膜，在两个方形 SRR 结构中间填充了石墨烯，由于石墨烯是二维材料其单层厚度约为 0.34 nm，在仿真中考虑多层石墨烯重叠放置，即在添加材料时选择 Graphene_Eps 材料。单元结构具体参数如下：结构单元周期 $P_x=P_y=100$ μm，$a=60$ μm，SRR 结构的宽度 $w_1=w_3=5$ μm，缺口宽度 $d=10$ μm，石墨烯的宽度 $w_2=5$ μm。各单元结构由宽度为 1 μm 的条状金薄膜横向连接以便于对整个阵列施加偏置电压，该电极结构对本文仿真结果影响很小，因此在后面的示意图中，忽略金属条[22]。为了研究该结构的性能，本文使用全波电磁软件 CST 微波工作室 2019 实现频域仿真，基于有限积分法（FIT）实现对离散 Maxwell 方程求解。在仿真条件上选择在 x 和 y 方向设置 unit cell 边界条件，$+z$ 方向设置 open and space 边界，$-z$ 方向设置 open 边界。

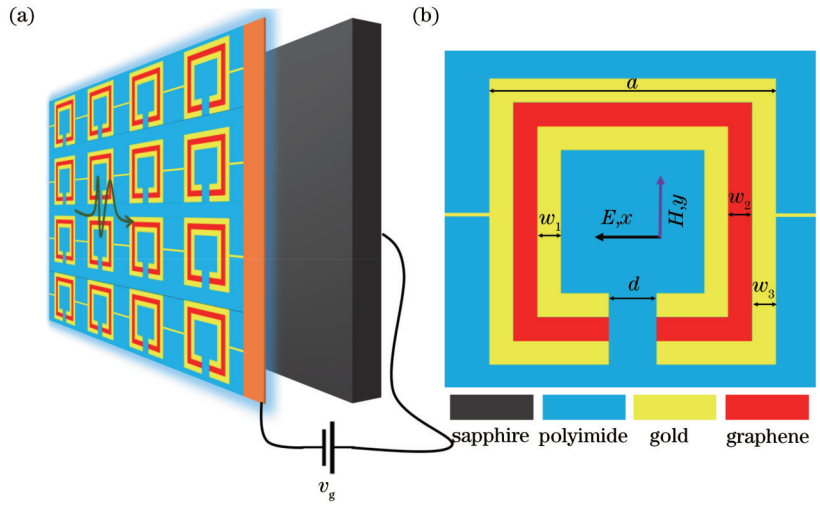

图 1　石墨烯超表面结构示意图。(a) 4×4 阵列；(b) 俯视图

Fig. 1　Schematic diagram of graphene metasurface structure. (a) 4×4 array; (b) top view

石墨烯的电导率用 Kubo 公式可以描述为带内电导率 δ_{intra} 和带间电导率 δ_{inter} 之和。它们都是由电子跃迁贡献，而在太赫兹频段内电磁波能量远远低于受共价键束缚的电子发生能级跃迁需要的能量，即 $E_f\gg\hbar\omega$，因此不考虑带内电导率的贡献从而得到了石墨烯在太赫兹频段的近似电导率[23]，表示为

$$\delta\approx\delta_{\text{inter}}=\mathrm{j}\frac{e^2K_{\mathrm{B}}T}{\pi\hbar^2\left(\omega+\mathrm{j}\tau^{-1}\right)}\left\{\frac{E_{\mathrm{f}}}{K_{\mathrm{B}}T}+2\ln\left[\exp\left(\frac{-E_{\mathrm{f}}}{K_{\mathrm{B}}T}\right)+1\right]\right\},\tag{1}$$

式中：E_{f} 为费米能级；T 为温度，取 $T=300$ K；ω 为入射电磁波的角频率；τ 为弛豫时间，取 $\tau=0.1$ ps；K_{B} 为玻尔兹曼常数；$\hbar$ 为普朗克常量。$K_{\mathrm{B}}=\hbar\omega$ 为电磁波的能量，由于 $E_{\mathrm{f}}\gg\hbar\omega$，因此将式(1)中的对数项忽略得到了简化的石墨烯电导率

$$\delta\approx\mathrm{j}\frac{e^2E_{\mathrm{f}}}{\pi\hbar^2\left(\omega+\mathrm{j}\tau^{-1}\right)}。\tag{2}$$

式(2)中电导率为一个复数，记为 $\delta=\delta_{\mathrm{r}}+\mathrm{j}\delta_{\mathrm{i}}$，其可以通过调节费米能级的大小实现调控。在 0～40 THz 频段石墨烯电导率的实部和虚部如图 2 所示，可以看到：当费米能级不变时，石墨烯电导率实部逐渐减小，且在低频和高频段变化率较小，而虚部先增加后减小且在低频段变化率较大；随着费米能级的增加，石墨烯电导率的实部和虚部均增大。

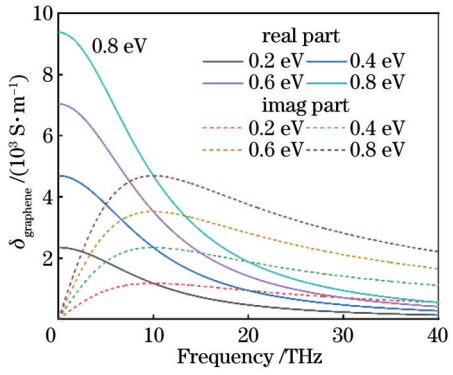

图 2　石墨烯电导率与频率和费米能级的关系

Fig. 2　Relationship between graphene conductivity and frequency at different Fermi levels

3　仿真结果与讨论

图 3(a)为未填充石墨烯时的透射频谱及谐振点的电场分布，可以看到在 0.824 THz 和 1.003 THz 处各有一个谐振点：在 0.824 THz 处的谐振点，其电场主要分布在外 SRR 结构 x 轴方向内外侧且电场强度较弱，这说明该点主要由外 SRR 结构与电磁波耦合形成表面等离激元且耦合程度较弱；在 1.003 THz 处的谐振点其电场主要分布在内 SRR 结构 x 轴方向内外侧，

其电场强度明显增强，说明该点主要由内SRR结构与电磁波耦合形成表面等离激元且耦合程度较强。由于结构尺寸、与入射波耦合程度和耦合频率均不同，该结构在不同位置处发生明模共振，内SRR结构被强激发，外SRR结构被弱激发。图3(b)为填充石墨烯后不同结构的透射光谱，内SRR结构与石墨烯耦合在1.004 THz处激发了偶极子谐振，外SRR结构与石墨烯耦合在1.023 THz也激发了偶极子谐振。相对地，前者谐振强度较弱可以看作“暗模式”，后者可以看作明模式。将两个子谐振器耦合后发生干涉并成功激发了PIT效应，在0.929 THz和1.037 THz处各有一个谐振点，记为dip A和dip C，在1.016 THz处有一个透射峰记为peak B。为了探究PIT效应的物理机理，图4为各点的电场及表面电流分布。如图4(a)、(c)所示，在谐振点dip A和dip C处明暗模式能够分别以不同程度被电磁波激发，dip A与dip C的电场分布位置相同，均分布在远离石墨烯的一侧。结合图4(d)、(f)可以看到：dip A被强激发且在金属环上产生了方向相同的表面电流；dip C被弱激发且在金属环上产生了方向相反的表面电流。如图4(b)、(e)所示，在peak B处明暗模式发生干涉，原有的电磁辐射场相互抵消使得电场分布减弱，且peak B与dip A的表面电流均为同向分布，这与dip A处谐振被强激发一致。从模式杂化的角度出发，谐振点是由于明暗模式杂化产生了两种集体谐振模式，即dip A处产生了高能反键模式，dip C处产生了低能键合模式[24]。

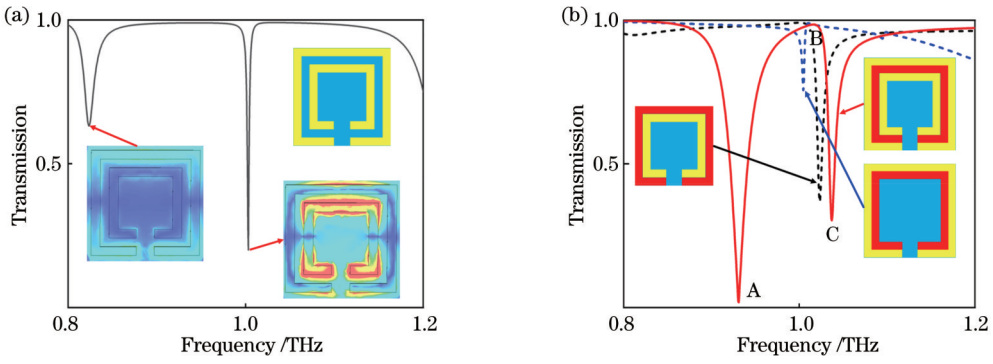

图3　超表面透射频谱。(a)未填充石墨烯；(b)填充石墨烯

Fig. 3　Metasurface transmission spectrum. (a) Unfilled with graphene;(b) filled with graphene

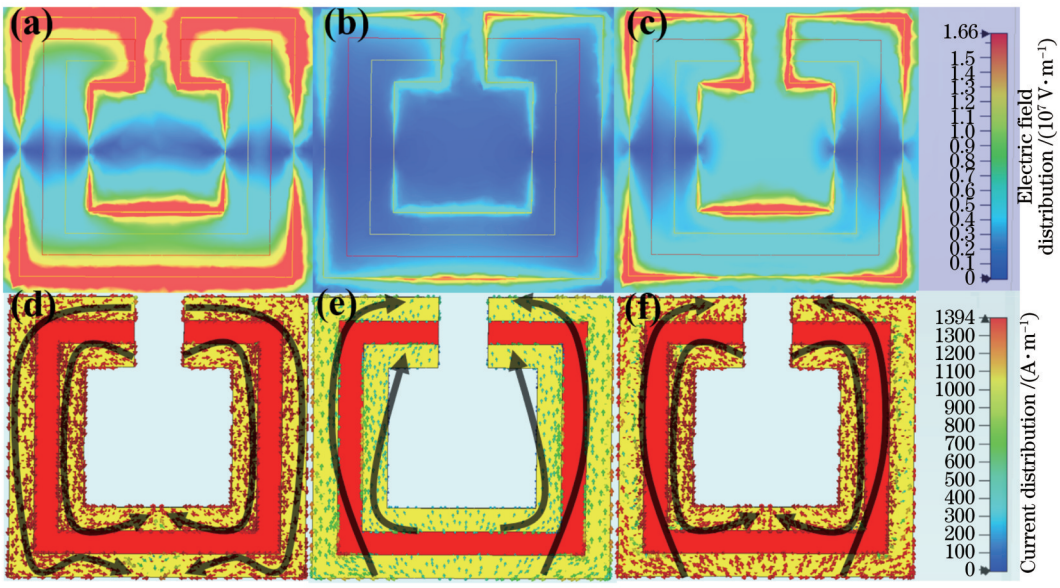

图4　PIT效应物理机理。(a) dip A电场分布，f=0.929 THz；(b) peak B电场分布，f=1.016 THz；(c) dip C电场分布，f=1.037 THz；(d) dip A电流分布；(e) peak B电流分布；(f)dip C电流分布

Fig. 4　Physical mechanism of PIT. (a) Electric field distribution at dip A, f=0.929 THz; (b) electric field distribution at peak B, f=1.016 THz; (c) electric field distribution at dip C, f=1.037 THz; (d) current distribution at dip A; (e) current distribution at peak B; (f) current distribution at dip C

石墨烯的加入使得该结构具有了动态可调性，图5(a)为费米能级在0.2 eV到1 eV变化时的透射频谱，可以看到其主要实现了对谐振点透射率的调制，透射频率几乎不受影响。为了量化调制特性，如图5(b)所

示：dip A的谐振频率稳定在0.928 THz处，dip C的频率稳定在1.0367 THz处；dip A和dip C的透射率均与费米能级的大小呈负相关，随着费米能级的大小从0.2 eV增加到1.0 eV，dip A的透射率下降了约36.84%，而dip C的透射率下降了约47.87%。设谐振点处的最大调制深度为$(T_{max}-T_{min})/T_{max}\times100\%$，则dip A和dip C处的最大调制深度分别为96.05%和65.40%。

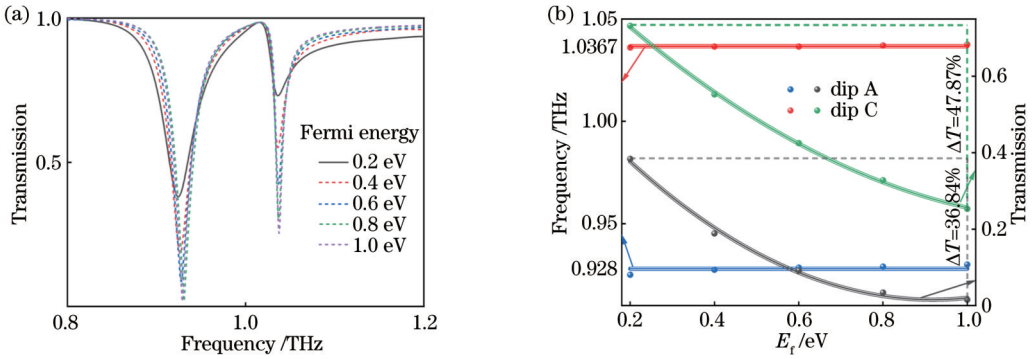

图5　费米能级的动态调控。(a)不同费米能级下的透射频谱。(b)费米能级对谐振的影响

Fig. 5　Dynamic control by the Fermi levels. (a) Transmission spectrum at different Fermi levels; (b) influence of Fermi levels on resonance

目前对石墨烯调控方式主要是通过外加偏置电压或者直接掺杂载流子两种方式，其中外加偏置电压因其具有高调制深度、低损耗和功能多样等优点逐渐成为主流，该工作原理可等效为电容耦合电路。电控石墨烯的结构与场效应管类似，当石墨烯层施加正偏压、蓝宝石衬底施加负偏压时，电子积聚在石墨烯层形成n掺杂，反之则是p掺杂，而中间的介质层起到隔绝电子移动的作用从而使石墨烯层与绝缘层形成了电容器结构。如图6(a)所示，最上层的金薄膜与石墨烯可以看成是并联的电容器，然后再与聚酰亚胺电容器形成串联，设三者的总电容为C_{total}，则

$$C_{total}=\frac{1}{\frac{1}{C_{gold}+C_{graphene}}+\frac{1}{C_{polyimide}}}。\tag{3}$$

各结构的电容$C=\frac{\varepsilon_0\varepsilon_r}{d}$，其中，$d$为材料的厚度，$\varepsilon_r$为材料相对介电常数。设绝缘层的厚度为50 nm，可以算出$C_{polyimide}=6.198\times10^{-4}$F/m。由式(2)可得到石墨烯电导率的实部和虚部，根据$\varepsilon_{graphene}=-\frac{\delta_i}{\varepsilon_0\omega d}$可以算出石墨烯相对介电常数的实部，金的介电常数可以用drude模型描述为$\varepsilon(\omega)=\varepsilon_\infty-\frac{\omega_p^{\ 2}(\delta)}{\omega^2+j\omega\gamma}$，其中，$\varepsilon_\infty=5.967$为高频相对介电常数，$\omega_p^{\ 2}(\delta)=\frac{\delta}{\delta_0}\omega_p^{\ 2}(\delta_0)$为等离子体频率，$\delta_0=3\times10^5$ S/m，$\omega_p(\delta_0)=1.4\times10^{15}$ rad/s，$\gamma=5.75\times10^{13}$ rad/s为碰撞频率。由此分别得到了石墨烯和金在0.8～1.2 THz频段的介电常数的实部如图6(b)、(c)所示，可以看到它们的介电常数实部与聚酰亚胺最多相差了10^4数量级，根据电容串联规则可以将式(3)化简为$C_{total}\approx C_{polyimide}=6.198\times10^{-4}$ F/m。根据载流子浓度与偏置电压关系$n=\frac{C_{total}V_g}{e}$和费米能级公式$E_f=\omega\sqrt{n\pi}$可得到费米能级和偏置电压的关系，

$$E_f=\hbar V_f\sqrt{\frac{\pi C_{total}V_g}{e}},\tag{4}$$

式中：$V_f=1.1\times10^6$ m/s为费米速度；V_g为偏置电压。

从图6(a)可以看到，偏置电压与石墨烯费米能级呈正相关且变化率在减小。由此得到了偏置电压对谐振点透射率的影响，如图7(a)所示，可以看到电压只对谐振点振幅实现了调制，谐振频率几乎不变。为了实现对谐振频率的调制，本文考虑对结构参数进行优化。如图7(b)所示，通过改变石墨烯的宽度可以实现谐振点的频移，随着石墨烯宽度的减小dip A和dip C的谐振频率均出现不同程度的红移，但两个谐振点的距离增加。同时注意到谐振点的透射率随石墨烯宽度减小而降低，这是由于透射率的大小与谐振强度呈正相关，石墨烯宽度减小使得两个子谐振器自身的谐振强度减弱，从而发生干涉后在谐振点处透射率减小。

慢光效应指光在介质中的群速度慢于真空中光速的现象，具有PIT效应的结构在透明窗口处往往同时满足慢光效应需要的条件，即高色散和低吸收损耗。一般用群延时$\tau_g=\mathrm{d}\varphi(\omega)/\mathrm{d}\omega$来描述慢光特性，其中$\varphi(\omega)$为相位谱。基于前文的电压调控可得到如图8(a)所示的0～50 V电压下群延时曲线。可以看出，0.8～1.2 THz频段有3个群延时较高的点，其中群延时最高的点是PIT透明窗峰值处，并且群延时与偏置电压呈正相关。量化偏置电压对PIT透明窗峰值处群延时的影响如图8(c)所示，偏置电压与群延时关系的规律性较强，拟合系数$R^2=0.999$，电压从0～50 V变

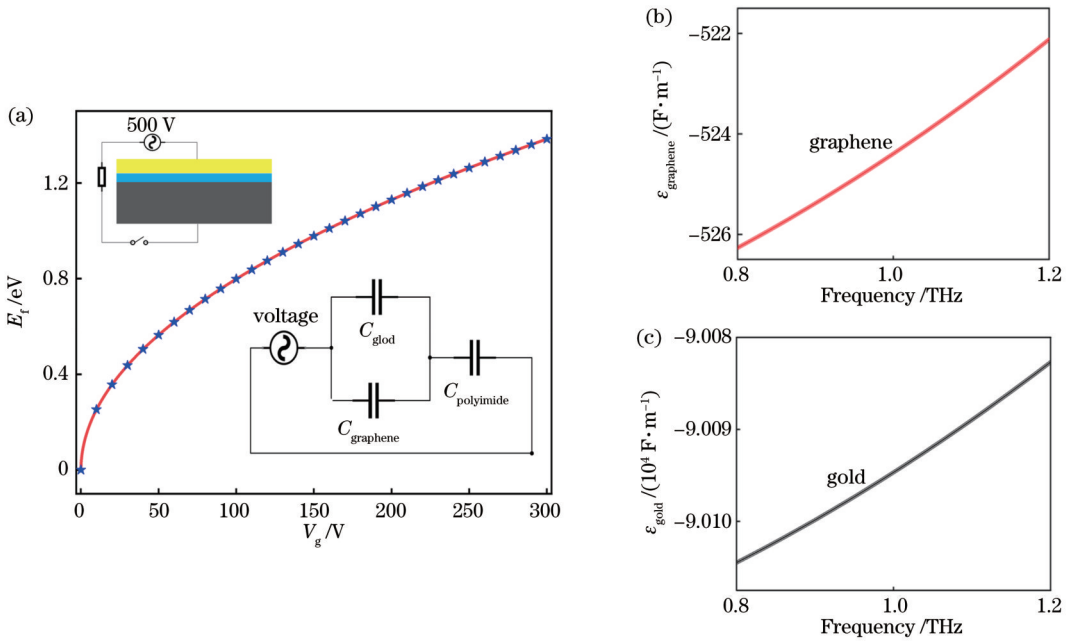

图 6　电压调制。(a)费米能级与偏置电压关系;(b)石墨烯介电常数实部与频率关系;(c)金介电常数实部与频率关系

Fig. 6　Voltage modulation. (a) Relationship between Fermi levels and bias voltages; (b) relationship between graphene dielectric constant real part and frequency; (c) relationship between gold dielectric constant real part and frequency

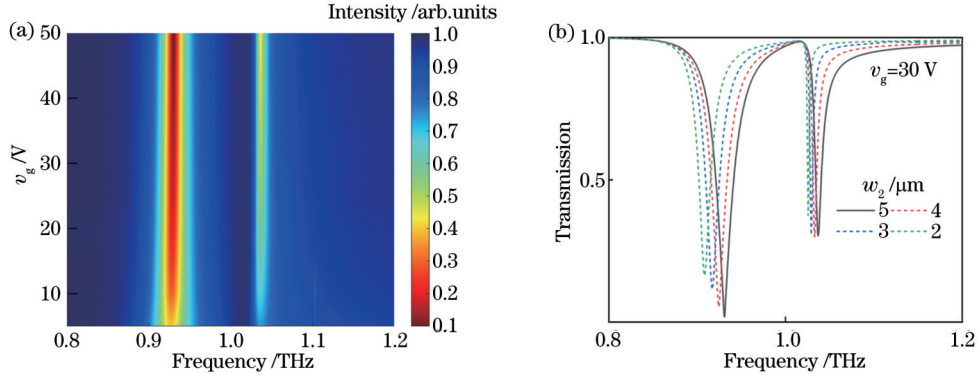

图 7　对结构透射光谱的调制。(a)电压调制;(b)石墨烯宽度调制

Fig. 7　Modulation of structural transmission spectra. (a) Voltage modulation; (b) graphene width modulation

化时群延时从 14.3 ps 变化到 44.11 ps 共增加了 29.81 ps。群折射率 n_g 的值也能反映慢光特性的优劣,一般群折射率越大结构的慢光效应越明显,

$$n_g = n_{eff} + \omega \frac{dn_{eff}}{d\omega}, \tag{5}$$

式中:n_{eff} 为结构的等效折射率。可以利用 S 参数反演法求出,其计算公式为

$$n_{eff} = \frac{1}{kd} \arccos\left(\frac{1 - S_{11}^2 + S_{21}^2}{2S_{21}}\right), \tag{6}$$

式中:k 为电磁波的波数;d 为材料的厚度;S_{11} 和 S_{21} 分别是反射系数和透射系数。由此得到了不同电压下结构的群折射率,如图 8(b)所示,可以看出,群折射率的实部在 dip A 和透射峰 peak B 处出现了峰值,dip A 处峰值约为 792,这说明光通过该结构所用时间是真空中的 1/792,充分证明了该结构对光的缓存作用。此外延时带宽积(DBP)也是衡量慢光器的重要指标之一,其定义为最大群延时透射窗带宽的乘积,即 $B_{DP} = \tau_g \times \Delta f$,如图 11(d)所示,偏置电压与 DBP 关系的规律性较强,拟合系数 R^2=0.996,电压从 0~50 V 变化时 DBP 从 0.34 变化到 3.66 共增加了 3.32。品质因子(Q)值是谐振腔的关键参数之一,其表征着光在传输过程的中的损耗程度,一般来说 Q 值越大结构的损耗越小,因此 Q 值的大小也是评价慢光器件的重要影响因素之一。其定义为 $Q = \frac{f_0}{\Delta f}$,f_0 是透射峰的共振频率,Δf 是透射峰窗口的最大半宽度。

为了研究 PIT 透射窗峰值处的色散特性,本文分别研究了偏置电压 V_g 对透射峰处群延时、群折射率、DBP 和 Q 值的影响,如表 1 所示,可以看到,群延时、群折射率和 DBP 与偏置电压均呈正相关,Q 值与偏置电

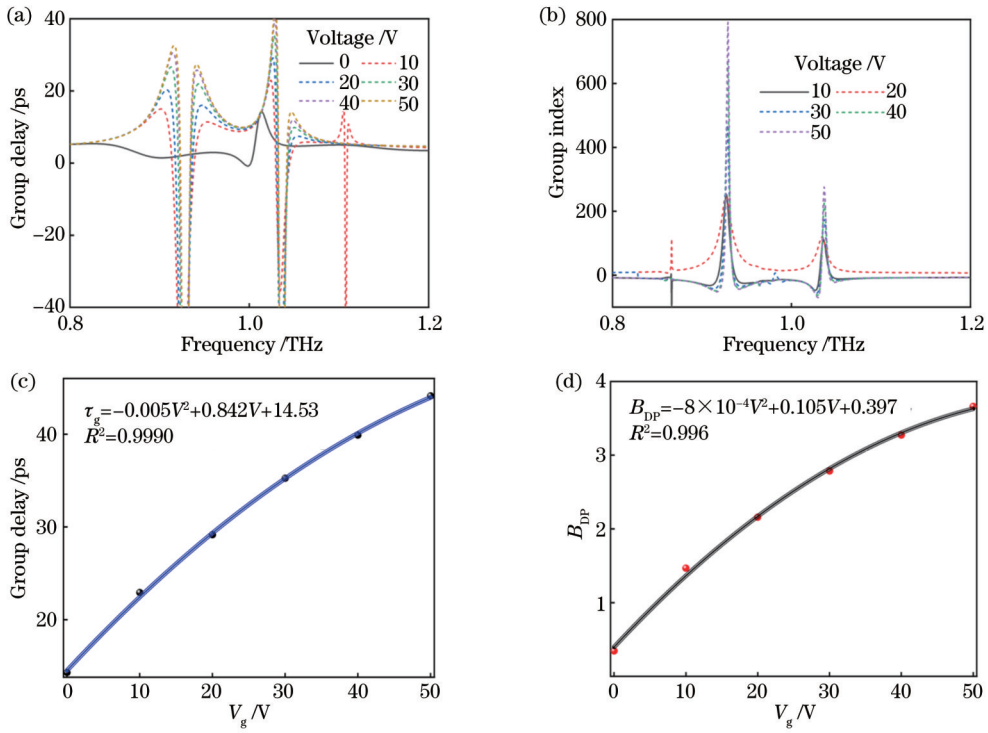

图 8　慢光效应的动态可调性。(a)群延时;(b) 群折射率;(c) 群延时与偏置电压的关系;(d) 延时带宽积与偏置电压的关系

Fig. 8　Dynamic adjustability of the slow light performance. (a) Group delay; (b) group index; (c) relationship between group delay and bias voltage; (d) relationship between the delay bandwidth product and the bias voltage

表 1　偏置电压对慢光效应的影响

Table 1　Influence of bias voltage on slow light performance

Voltage /V	Group delay /ps	Group index	DBP	Q value
0	14.30	−22.54	0.34	42.33
10	22.92	106.96	1.47	15.88
20	29.15	107.01	2.16	13.73
30	35.25	173.90	2.78	12.86
40	39.89	225.09	3.27	12.39
50	44.11	276.19	3.66	12.24

压呈负相关。这说明低损耗和高色散特性不能同时满足。值得注意的是,当未加偏置电压时,透射峰处的群折射率为负值,这并不说明此时电磁波通过材料的速度超过了光速,而是振幅包络线无延时通过超材料的现象。结构参数同样能够影响结构的慢光效应,当偏置电压 V_g=30 V 时石墨烯宽度 w_2 对结构慢光效应的影响如表 2 所示。可以看到,群延时、群折射率和 DBP 与石墨烯宽度均呈负相关,Q 值与石墨烯宽度呈正相关。表 3 展示了本文所提结构与其他结构的性能比较,可以看到,本文所提结构的群折射率和延时带宽积参数的性能明显优于其他结构,群延时低于文献[26],但其设计的结构不具有动态可调性,在实际应用中局限性较大。综合考虑,本文设计的慢光器件性能相较于其他的结构具有显著的优势。

表 2　V_g=30 V 时石墨烯宽度对慢光效应的影响

Table 2　Influence of graphene width on slow light performance when V_g=30 V

w_2 /μm	Group delay /ps	Group index	DBP	Q value
5	35.25	173.90	2.78	12.86
4	47.09	290.68	4.02	11.94
3	66.76	435.90	6.19	11.01
2	93.12	756.67	9.31	10.19

表 3　本文所提结构与其他结构的慢光效应性能比较

Table 3　Comparison of slow light performance between proposed structure and other structures

Ref.	Group delay /ps	Group index	DBP	Adjustability (Y/N)
[25]	31.35	30	0.62	Y
[26]	**614.00**	103	0.45	N
[27]	0.16	52	0.82	N
[28]	—	26	0.31	Y
[29]	0.49	586	0.35	Y
Proposed	93.12	**757**	**9.31**	Y

4　结　　论

本文提出了一种金属-石墨烯耦合结构用来实现动态可调的 PIT 效应,该现象由明-明模式干涉相消形成。通过调节石墨烯的费米能级可以在 0.929 THz 和 1.037 THz 处实现振幅调制,最大调制深度分别为 96.05% 和 65.40%。通过等效电容耦合电路计算出

偏置电压与费米能级的关系可知，当偏置电压为30 V、石墨烯宽度为2 μm时，慢光效应中群延时、群折射率、DBP和Q值分别可达93.12 ps、756.67、9.31和10.19。本文研究结果在慢光器件制作、THz通信等领域具有重要的研究价值。

参 考 文 献

[1] Ogawa Y, Hayashi S, Oikawa M, et al. Interference terahertz label-free imaging for protein detection on a membrane[J]. Optics Express, 2008, 16(26): 22083-22089.

[2] Li Y Y, Chen X Y, Hu F R, et al. Four resonators based high sensitive terahertz metamaterial biosensor used for measuring concentration of protein[J]. Journal of Physics D: Applied Physics, 2019, 52(9): 095105.

[3] Zeng Q P, Liu W T, Lin S J, et al. Aptamer HB5 modified terahertz metasurface biosensor used for specific detection of HER2[J]. Sensors and Actuators B: Chemical, 2022, 355: 131337.

[4] Ergin T, Stenger N, Brenner P, et al. Three-dimensional invisibility cloak at optical wavelengths[J]. Science, 2010, 328(5976): 337-339.

[5] Xu R J, Liu X Y, Lin Y S. Tunable ultra-narrowband terahertz perfect absorber by using metal-insulator-metal microstructures [J]. Results in Physics, 2019, 13: 102176.

[6] 袁婷婷, 吴靖文, 薄艳华, 等. 基于太赫兹超表面传感器的硝基呋喃类药物痕量检测[J]. 光学学报, 2023, 43(7): 0717001.
Yuan T T, Wu J W, Bo Y H, et al. Trace detection of nitrofuran drugs based on terahertz meta-surface sensor[J]. Acta Optica Sinica, 2023, 43(7): 0717001.

[7] Xu J J, Liao D G, Gupta M, et al. Terahertz microfluidic sensing with dual-torus toroidal metasurfaces[J]. Advanced Optical Materials, 2021, 9(15): 2100024.

[8] Chen L, Liao D G, Guo X G, et al. Terahertz time-domain spectroscopy and micro-cavity components for probing samples: a review[J]. Frontiers of Information Technology & Electronic Engineering, 2019, 20(5): 591-607.

[9] Chen H T, Padilla W J, Zide J M O, et al. Active terahertz metamaterial devices[J]. Nature, 2006, 444(7119): 597-600.

[10] Shrekenhamer D, Chen W C, Padilla W J. Liquid crystal tunable metamaterial absorber[J]. Physical Review Letters, 2013, 110(17): 177403.

[11] 黄成成, 张永刚, 梁兰菊, 等. 窄/宽带可切换的石墨烯-二氧化钒复合结构太赫兹吸波器[J]. 光学学报, 2022, 42(19): 1916001.
Huang C C, Zhang Y G, Liang L J, et al. Narrow/broad band switchable terahertz absorber based on graphene and vanadium dioxide composite structure[J]. Acta Optica Sinica, 2022, 42(19): 1916001.

[12] Wu Y, La-o-vorakiat C, Qiu X P, et al. Graphene terahertz modulators by ionic liquid gating[J]. Advanced Materials, 2015, 27(11): 1874-1879.

[13] Mostaan S M A, Saghaei H. A tunable broadband graphene-based metamaterial absorber in the far-infrared region[J]. Optical and Quantum Electronics, 2021, 53(2): 96.

[14] Chen Y F, Pan X S, Bao Z Y, et al. Tunable terahertz perfect-absorbers with dual peak based on reverse graphene patch metamaterials[J]. IEEE Photonics Journal, 2021, 13(3): 4800312.

[15] Monfared Y E, Qasymeh M. Graphene-assisted infrared plasmonic metamaterial absorber for gas detection[J]. Results in Physics, 2021, 23: 103986.

[16] Zhao X L, Yuan C, Lü W H, et al. Plasmon-induced transparency in metamaterial based on graphene and split-ring resonators[J]. IEEE Photonics Technology Letters, 2015, 27(12): 1321-1324.

[17] Peng J, He X Y, Shi C, et al. Investigation of graphene supported terahertz elliptical metamaterials[J]. Physica E: Low-Dimensional Systems and Nanostructures, 2020, 124: 114309.

[18] Chen L, Xu N N, Singh L, et al. Defect-induced Fano resonances in corrugated plasmonic metamaterials[J]. Advanced Optical Materials, 2017, 5(8): 1600960.

[19] Patil C M, Arregui G, Mechlenborg M, et al. Observation of slow light in glide-symmetric photonic-crystal waveguides[J]. Optics Express, 2022, 30(8): 12565-12575.

[20] Zong X Y, Li L X, Liu Y F. Bound states in the continuum in all-van der Waals photonic crystals: a route enabling electromagnetically induced transparency[J]. Optics Express, 2022, 30(11): 17897-17908.

[21] Khattak M I, Ullah Z, Al-Hasan M, et al. Enhanced tunable plasmonic resonance in crumpled graphene resonators loaded with gate tunable metamaterials[J]. Optics Express, 2020, 28(25): 37860-37878.

[22] 杨森, 王佳云, 张婷, 等. 温度电压双可控宽带太赫兹极化转换/吸收超表面[J]. 光学学报, 2022, 42(8): 0824001.
Yang S, Wang J Y, Zhang T, et al. Temperature-voltage Bi-controllable broadband terahertz polarization conversion/absorption metasurface[J]. Acta Optica Sinica, 2022, 42(8): 0824001.

[23] Yu W, Meng H Y, Chen Z J, et al. The bright-bright and bright-dark mode coupling-based planar metamaterial for plasmonic EIT-like effect[J]. Optics Communications, 2018, 414: 29-33.

[24] Ling Y H, Huang L R, Hong W, et al. Polarization-controlled dynamically switchable plasmon-induced transparency in plasmonic metamaterial[J]. Nanoscale, 2018, 10(41): 19517-19523.

[25] Han L, Tan Q L, Gan Y, et al. Polarization-insensitive classical electromagnetically induced transparency metamaterial with large group delay by Dirac semimetal[J]. Results in Physics, 2020, 19: 103377.

[26] Bagci F, Akaoglu B. A polarization independent electromagnetically induced transparency-like metamaterial with large group delay and delay-bandwidth product[J]. Journal of Applied Physics, 2018, 123(17): 173101.

[27] Lu Q, Wang Z Z, Huang Q Z, et al. Plasmon-induced transparency and high-performance slow light in a plasmonic single-mode and two-mode resonators coupled system[J]. Journal of Lightwave Technology, 2017, 35(9): 1710-1717.

[28] Han Z H, Bozhevolnyi S I. Plasmon-induced transparency with detuned ultracompact Fabry-Perot resonators in integrated plasmonic devices[J]. Optics Express, 2011, 19(4): 3251-3257.

[29] Xiong C X, Chao L, Zeng B, et al. Dynamically controllable multi-switch and slow light based on a pyramid-shaped monolayer graphene metamaterial[J]. Physical Chemistry Chemical Physics, 2021, 23(6): 3949-3962.

Tunable Slow Light Performance Based on Graphene Metasurface

Ma Yi[1,2], Guo Jingyu[1,2], Chen Lin[1,2*]

[1]*School of Optical Electrical and Computer Engineering, University of Shanghai for Science and Technology, Shanghai* 200093, *China*;

[2]*Shanghai Key Laboratory of Modern Optical Systems, Shanghai* 200093, *China*

Abstract

Objective Plasmon-induced transparency (PIT) refers to an atypical transmission phenomenon that results from the coupling of various resonance modes with the near-field electromagnetic wave. This usually results in a slowdown of the speed of light at the transmission peak due to significant dispersion, which is known as slow light performance. Numerous studies have demonstrated that slow light performance can be achieved in optical fibers, waveguides, and metasurfaces, which has led to wide-ranging applications in areas such as optical storage and optical modulation. Metasurfaces offer several advantages over optical fibers and waveguides, including small size, ease of fabrication, and excellent electromagnetic properties. Moreover, the addition of graphene to metasurfaces provides high-quality properties such as high transmittance, low loss, and dynamical adjustability. As a result, graphene-based metasurfaces hold significant potential in the study of slow light performance. However, the production and utilization of complex patterned graphene are limited by the current state of nanomanufacturing technology. Therefore, studying the PIT effect in simple structures with high quality is crucial for the practical production and application of PIT devices in experiments and real-life settings. Moreover, designing simple and manufacturable structures that produce high-quality multi-mode PIT is of great significance to optical device fabrication. This will significantly promote the rapid development and application of photonic devices based on the PIT effect.

Methods In this paper, we investigate the PIT effect in monolayer patterned graphene metasurfaces using numerical simulations of the electromagnetic field. The simulations are performed using the full-wave electromagnetic software, namely CST Microwave Studio 2019, which utilizes the finite integration technique (FIT) to solve the discrete Maxwell equations. The metasurface structure consists of a split ring resonator (SRR) laterally coupled by metal-graphene-metal. Initially, we analyze the transmission spectrum and electric field distribution to gain insights into the PIT effect of the structure. Additionally, we derive a theoretical formula for graphene surface conductivity and investigate the effect of bias voltage on the dielectric constant of graphene by changing the Fermi level. Subsequently, we study the impact of different Fermi levels on amplitude modulation. Finally, we demonstrate the dynamic modulation of slow light performance by varying the bias voltage and graphene width.

Results and Discussions In this paper, we present the design and analysis of a monolayer patterned metal-graphene metasurface that achieves a high-quality PIT effect (Fig. 1). We observe that as the Fermi level of graphene increases, the transmittance at resonance points also increases. Specifically, we achieve amplitude modulations of 96.05% and 65.40% at two different resonance points (Fig. 5). To quantify the relationship between the bias voltage and the Fermi level of graphene, we propose an equivalent capacitive coupling model, which shows that graphene primarily modulates the amplitude and has low sensitivity to frequency. Resonance frequency modulation can be achieved by changing the structural parameters such as the width of graphene (Fig. 7). We evaluate the performance of the slow light effect using parameters such as group delay, group refractive index, and delay bandwidth product (DBP). We find that the bias voltage is positively correlated with these parameters, while the graphene width is negatively correlated with them. For instance, when the bias voltage is set to 50 V, and the graphene width is stable, we obtain group delay, group refractive index, and DBP values of 44.11 ps, 276.19, and 3.66, respectively (Table 1). By reducing the graphene width, we further optimize these parameters, resulting in group delay, group refractive index, and DBP values of 93.12 ps, 756.67, and 9.31, respectively (Table 2). The Q value characterizes the loss of the device, with a higher Q value indicating a lower loss. When no bias voltage is applied, we obtain the largest Q value of 42.33. However, the Q value gradually decreases as the bias voltage increases, or the graphene width decreases. This suggests that high dispersion and low loss characteristics cannot be simultaneously achieved and need to be balanced in practical applications. Finally, we compare our device with relevant studies and demonstrate its significant advantages.

Conclusions The study proposes a metal-graphene coupling structure to achieve a dynamically adjustable PIT effect,

which results from the interference cancellation of the bright-bright mode. By adjusting the Fermi level of graphene, amplitude modulation can be achieved at 0.929 THz and 1.037 THz, with maximum modulation depths of 96.05% and 65.40%, respectively. By using the equivalent capacitive coupling circuit, the relationship between the bias voltage and Fermi level is calculated, and it is found that a bias voltage drop of $V_g = 30$ V and graphene width of $w_2 = 2$ μm can result in group delay, group refractive index, DBP, and Q values of 93.12 ps, 756.67, 9.31, and 10.19, respectively. These results hold significant value in slow optical device fabrication, THz communication, and detection research.

Key words plasmon-induced transparency; graphene; tunable; slow light effect; terahertz